Research Article

Analytical study for MHD flow of Williamson nanofluid with the effects of variable thickness, nonlinear thermal radiation and improved Fourier's and Fick's Laws

SN

Sumit Gupta[1] · Devendra Kumar[2] · Jagdev Singh[3] (iD)

Abstract

The key aim of the present work is to analyze the magnetohydrodynamic 2D flow of Williamson type nanofluid. Heat and mass transfer impacts are carried out in the manifestation of nonlinear thermal radiation, Cattaneo–Christov heat and mass flux models and varying thicker surface. By applying the appropriate similarity transformations, the mathematical equations of velocity, temperature and volume fraction transform to NODEs. An analytical scheme is pragmatic to estimate the convergence solutions in terms of power series. The dimensionless velocity profile, temperature profile and nanoparticle volume fraction with the administrative physical aspects are depicted through graphs. It is evidently ostensible that the dimensionless velocity declines for the augmented index parameter and wall thickness while cumulative values of M and β, the horizontal fluid velocity decreases. Temperature specie upsurges with rising of $Nb, Nt, n, \beta, R_d, \theta_w$ and M. Consequently demotes with the higher values of Pr and De_1. Nanoparticle volumetric specie escalates with the growing effects of Nt, while it diminishes with Nb, Sc and De_2. Comparison is the key procedure for validation our results with the earlier literature.

1 Introduction

Nanofluids is the name discovered by Choi [1] to interpret this novel class of nanoparticles based fluids that demonstrates thermal inheritances higher-up to those of their base fluids. Due to their small size usually less than 100 nm, nanoparticles fluidize simply in the base fluid and as a result, clogging and erosion in channels are no longer a problem. These particles carry only a few thousand atoms and own properties that are substantially differ from their original materials. Recently there have been several advancements which have made the nanofluids more stable and ready for use. Nanofluids find potential applications in electronic devices as they have higher denser chips with compact design which makes heat dissipation difficult, heat pipes in the computer devices to improve heat dissipation, industrial cooling using resulting in excellent energy savings and emission reduction, for cooling nuclear systems, space and defense because of the restriction of space and heat exchangers to improve heat transfer rates, in fuel cell, Solar water heaters, chillers, domestic refrigerator and as lubricants in machining.

Nanofluids are not merely liquid–solid amalgams but are composed by dispersing nanometer-scale solid particles into

✉ Jagdev Singh, jagdevsinghrathore@gmail.com; Sumit Gupta, guptasumit.edu@gmail.com; Devendra Kumar, devendra.maths@gmail.com | [1]Department of Mathematics, Swami Keshvanand Institute of Technology, Management and Gramothan, Ramnagaria, Jaipur, Rajasthan 302017, India. [2]Department of Mathematics, University of Rajasthan, Jaipur, Rajasthan 302004, India. [3]Department of Mathematics, JECRC University, Jaipur, Rajasthan 303905, India.

the base liquids such as water, oils, ethylene glycol, etc. It is well known that the metal nanoparticles oxidize in the process of preparation and their high density paved the path for the simple sedimentation. It is observed that the oxide nanoparticles are found chemically stable and are simple to generate and disperse in the process of preparation. Among the oxides Al_2O_3 nanoparticles find in major applications and exhibit less wear and friction properties in comparison of the others apart from higher thermal conductivity and low density. Consequently, Al_2O_3 nanoparticles are chosen for the present investigation. Base fluids generally employed in the production of nanofluids are the well-known working fluids in heat transfer practices; such as water, engine oil and ethylene glycol. Therefore, Al_2O_3- water nanofluids are suitable for cooling applications in the automotive industry. In the present work Al_2O_3 nanoparticles are dispersed in de-ionized water (here after referred to as water) in fraction of volume.

The nanofluid have been investigated both theoretical as well as experimental accomplishments [2–19]. Sheikholeslami et al. [20] discussed an experimental study on use of nano-refrigerant for boiling heat transfer enrichment. In an article Sheikholeslami et al. [21] also elaborated the heat transfer enhancement with turbulator and entropy generation. Some remarkable work on the energy storage and entropy generation can be cited in [22–25]. Jha and Malgwi [26] investigated the combined effects of slip current and Hall on MHD flow in a vertical microchannel with free convection. Dabe et al. [27] examined Von Karman similarity transformation to evaluate the heat and mass transfer features on MHD power law fluid. Kumar et al. [28] discussed the stagnation point flow for the Williamson and Casson fluid with new heat flux model.

Our key objective is to examine the MHD flow of Williamson nanofluid confined by the stretching sheet with the variable thickness. Heat and mass transfer phenomena is inspected by nonlinear thermal radiation and Cattaneo–Christov heat and mass flux principles. Impact of Brownian motion (BM) and Thermophoresis diffusion (TD) are also discussed. The transformed boundary layer approximations for velocity, energy and concentrations are contemplated by the homotopy analytic method (HAM). Some prominent literature on the HAM are [29–47] and the references therein. The dimensionless velocity, temperature and nanoparticles concentration are discussed in the form of graphs in view of several governing parameters.

2 Mathematical formulations

Here we examine the steady MHD two dimensional (2-D) laminar Williamson nanofluid flow owing to stretching surface with variable thickness given by $y = \delta^*(x + b)^{\frac{1-n}{2}}$.

A varying magnetic field (MF) $B(x) = B_0(x + b)^{\frac{(n-1)}{2}}$ is taken in y-direction. Impact of viscous dissipation, slip condition and induced magnetic field are not deliberated for the flow. Features of heat, mass transfers are inspected by using the concept of Cattaneo–Christov heat/mass fluxes and nonlinear thermal radiation. Natures of nanoparticles are determined by noting the effects of BM and TD. Velocity of the surface is $U_w(x) = a_1(x + b_1)^{n^*}$, here a_1 and b_1 denotes the dimensional constants. The Fig. 1 demonstrates the coordinate system and flow regime.

The upper convective material derivative of any vector can be represent as

$$\frac{DA_1}{Dt} = \frac{\partial A_1}{\partial t} + V_1 \cdot \nabla A_1 - A_1 \cdot \nabla V_1 + (\nabla \cdot V_1) \cdot A_1 \qquad (1)$$

In Eq. (1) V_1 denotes the velocity vector while A_1 be extra vector that regraded for the heat or mass flux vector. Therefore the Cattaneo–Christov indifferent diffusion model are presented as

$$q + \lambda_1 \left[\frac{\partial q}{\partial t} + V_1 \cdot \nabla q - q \cdot \nabla V_1 + (\nabla \cdot V_1) \cdot q \right] = -k_f \nabla T$$
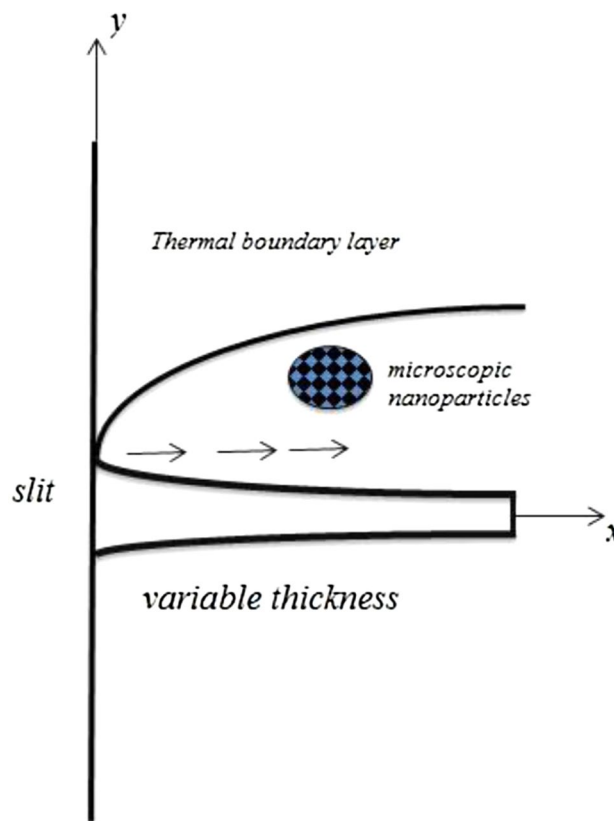
$$(2)$$

Fig. 1 Diagram of the problem

and

$$N + \lambda_2\left[\frac{\partial N}{\partial t} + V_1 \cdot \nabla N - N \cdot \nabla V_1 + (\nabla \cdot V_1) \cdot N\right] = -D_B\nabla C \tag{3}$$

In the Eqs. (1)–(3) q be the normal heat flux, N be the normal mass flux, k_f is the thermal conductivity (TC) of the fluid, D_B is the Brownian diffusion coefficient (BDC), λ_1 is the relaxation time due to heat flux, λ_2 is the relaxation time because of mass flux, $\frac{D}{Dt}$ is the material derivative and ∇ is the differential operator of the vector function. In the case of steady laminar flow we have $\frac{\partial q}{\partial t} = 0$, $\frac{\partial N}{\partial t} = 0$ and assuming $\nabla \cdot V = 0$ the above equation can be rewritten as

$$q + \lambda_1\left[V_1 \cdot \nabla q - q \cdot \nabla V_1\right] = -k_f\nabla T \tag{4}$$

$$N + \lambda_2\left[V_1 \cdot \nabla J - J \cdot \nabla V_1\right] = -D_B\nabla C \tag{5}$$

Upon using the following assumptions the ruling equations of the problem are presented by

$$\frac{\partial u^*}{\partial x} + \frac{\partial v^*}{\partial y} = 0 \tag{6}$$

$$u^*\frac{\partial u^*}{\partial x} + v^*\frac{\partial u^*}{\partial y} = \upsilon\frac{\partial^2 u^*}{\partial y^2} + \sqrt{2}\,\upsilon\,\Gamma\frac{\partial u^*}{\partial y}\frac{\partial^2 u^*}{\partial y^2} - \frac{\sigma^* B_0^2}{\rho_f} \tag{7}$$

$$u^*\frac{\partial T^*}{\partial x} + v^*\frac{\partial T^*}{\partial y} = \frac{k_f}{(\rho c_p)_f}\frac{\partial^2 T^*}{\partial y^2} - \lambda_1\left[\begin{array}{l}\left(u^*\frac{\partial u^*}{\partial x} + v^*\frac{\partial u^*}{\partial y}\right)\frac{\partial T^*}{\partial x} + \left(u^*\frac{\partial u^*}{\partial x} + v^*\frac{\partial u^*}{\partial y}\right)\frac{\partial T^*}{\partial y} + u^{*2}\frac{\partial^2 T^*}{\partial x^2}\\ +2u^*v^*\frac{\partial^2 T^*}{\partial x\partial y} + v^{*2}\frac{\partial^2 T^*}{\partial y^2}\end{array}\right]$$
$$-\frac{1}{(\rho c_p)_f}\frac{\partial q_r}{\partial y} \tag{8}$$

$$u^*\frac{\partial C^*}{\partial x} + v^*\frac{\partial C^*}{\partial y} = D_B^*\left(\frac{\partial^2 C^*}{\partial x^2} + \frac{\partial^2 C^*}{\partial y^2}\right) - \lambda_3\left[\begin{array}{l}\left(u^*\frac{\partial u^*}{\partial x} + v^*\frac{\partial u^*}{\partial y}\right)\frac{\partial C^*}{\partial x} + \left(u^*\frac{\partial u^*}{\partial x} + v^*\frac{\partial u^*}{\partial y}\right)\frac{\partial C^*}{\partial y} + u *^2\frac{\partial^2 C^*}{\partial x^2} + v *^2\frac{\partial^2 C^*}{\partial y^2}\\ +2u^*v^*\frac{\partial^2 C^*}{\partial x\partial y}\end{array}\right]$$
$$+\frac{D*_T}{T_\infty}\left(\frac{\partial^2 T^*}{\partial y^2}\right), \tag{9}$$

Along with the subsequent boundary conditions (BCs):

$$u^* = U_w(x) = a_1(x + b_1)^{n*}, \ v^* = 0, \ T^* = T_w, \ C^* = C_w \quad \text{at} \quad y = \delta(x + b_1)^{\frac{(1-n*)}{2}} \tag{10}$$
$$u^* \to 0, \quad v^* \to 0, \quad T^* \to T_\infty, \quad C^* \to C_\infty \quad \text{at} \quad y \to \infty$$

In the Eqs. (6)-(10) u^* and v^* are the components of the velocity, υ is standing for the kinematic viscosity, ρ_f is the density of the fluid, $(c_p)_f$ is the heat capacity at uniform pressure, σ is the electrical conductivity, B is the magnetic

field, T^* and C^* are standing for the fluid temperature and nanoparticle fraction respectively, T_w and T_∞ are indicating the temperature of the fluid at the wall and ambient boundary, D_B^* and D_T^* are respectively the Brownian motion and thermophoretic diffusion coefficient (TDC), $\tau^* = \frac{(\rho c_p)_p}{(\rho c_p)_f}$ is the ratio of the effective heat capacity of nanoparticles and base fluid, λ_1 and λ_2 are respectively heat and mass flux relaxation parameters and n^* is the power index.

Heat flux by Rosseland theory is presented as

$$q_r = -\frac{4\sigma}{3k^*}\frac{\partial T^{*4}}{\partial y} \tag{11}$$

In Eq. (11) σ stands for the Stefan–Boltzmann constant and k^* shows mean absorption coefficients.

On employing the subsequent similarity transformations

$$\psi = \sqrt{\frac{2}{(n*+1)}a_1\upsilon(x + b_1)^{n*+1}}\,f,$$

$$\zeta = \sqrt{\frac{(n*+1)a_1(x + b_1)^{n*+1}}{2\upsilon}}\,y,$$

$$\theta = \frac{T^* - T_\infty}{T_w - T_\infty}, \quad \phi = \frac{C^* - C_\infty}{C_w - C_\infty}, \tag{12}$$

$$T^* = T_\infty\left(1 + (\theta_w - 1)\theta\right), \quad u^* = a_1(x + b_1)^{n*}f,$$

$$v^* = -\sqrt{\frac{(n*+1)a_1\upsilon(x + b_1)^{n*-1}}{2}}\left[f + \zeta\left(\frac{n*-1}{n*+1}\right)f'\right] \tag{13}$$

The Eq. (6) trivially holds while other equations give [45]

$$f''' + f f'' + \beta_1 f'' f''' - \frac{2n^*}{n^* + 1} f'^2 - \frac{2}{n^* + 1} M^2 f' = 0 \quad (14)$$

$$\left(1 + \frac{4}{3} R_d\right)\theta'' + \frac{4}{3} R_d \big[(3\theta^2\theta'^2 + \theta^3\theta'')(\theta_w - 1)^3$$
$$+ 3(2\theta'^2\theta + \theta^2\theta'')(\theta_w - 1)^2 + 3(\theta'^2 + \theta\theta'')(\theta_w - 1)\big]$$
$$+ \Pr\big[f\theta' + De_1(f f''\theta + f f'\theta' - f'^2\theta - f^2\theta'')\big] = 0$$
$$(15)$$

$$\phi'' + Sc\big[f\phi' + De_2(-f'^2\phi + f f''\phi - f^2\phi'' + f f'\phi')\big] + \frac{N_t}{N_b}\theta'' = 0$$
$$(16)$$

With the subsequent boundary conditions (BCs):

$$f' = 1, \quad f = \alpha\left(\frac{1 - n^*}{1 + n^*}\right), \quad \theta = 1, \quad \phi = 1 \quad \text{at} \quad \zeta = 0$$
$$f' \to 0, \quad \theta \to 0, \quad \phi \to 0 \quad \text{at} \quad \zeta \to \infty$$
$$(17)$$

In the above equations M indicates the magnetic parameter (MP), β_1 represents the non-Newtonian parameter (NNP), R_d stands for the radiation parameter (RP), θ_w indicates the temperature parameter, Pr stands for the Prandtl number (PN), N_b is the Brownian motion parameter (BMP), N_t is the thermophoresis parameter (TP), Sc represents the Schmidt number (SN), De_1 indicates the Deborah number (DN) in terms of heat flux relaxation time, De_2 is the Deborah number (DB) in terms of mass flux relaxation time, respectively and are described as

$$M^2 = \frac{\sigma B^2(x)}{a_1 \rho}, \quad R_d = \frac{16\sigma^* T_\infty^3}{3k^* k_f}, \quad \theta_w = \frac{T_f}{T_\infty},$$
$$\Pr = \frac{(\mu c_p)_f}{k_f}, \quad N_t = \frac{\tau D_T(T_w - T_\infty)}{\upsilon T_\infty}, \quad Sc = \frac{\upsilon}{D_B},$$
$$De_1 = \lambda_1 a_1 n^*, \quad De_2 = \lambda_2 a_1 n^*, \quad N_b = \frac{\tau D_B(C_w - C_\infty)}{\upsilon}$$
$$(18)$$

Skin friction coefficients (SFC) C_{fx} and the LNN Nu_x are presented as

$$C_{fx} = \frac{\tau_w}{\rho U_w^2}, \quad Nu_x = \frac{(x + b_1)q_w}{k_f(T_f - T_\infty)} \quad (19)$$

where τ_w stands for the surface shear stress and q_w be the surface heat flux i.e.

$$\tau_w = \left[\upsilon\left(\frac{\partial u}{\partial y}\right) - \lambda_1\left(\upsilon\frac{\partial^2 u}{\partial y^2} + u\frac{\partial^2 u}{\partial x \partial y} - 2\frac{\partial u}{\partial x}\frac{\partial u}{\partial y}\right)\right]_{y=\delta(x+b_1)^{\frac{(1-n^*)}{2}}},$$
$$q_w = \left(\frac{\partial T}{\partial y}\right)_{y=\delta(x+b_1)^{\frac{(1-n^*)}{2}}}$$
$$(20)$$

Finally the skin friction and the LNN are given as follows

$$\frac{1}{2}\sqrt{Re_x} C_{fx} = \sqrt{\frac{(n+1)}{2}}\left((1 - 3\lambda_1)f''(0) + \frac{\beta_1}{2}f''(0)^2\right) \quad \text{and}$$

$$\frac{Nu_x}{\sqrt{Re_x}} = -\sqrt{\frac{(n+1)}{2}}\left(1 + \frac{4R_d}{3}(1 + (\theta_w - 1)\theta(0))^3\right)$$
$$(21)$$

In the above equations $Re_x = \frac{U_w(x+b)}{v_f}$ is indicating the local Reynold's number (LRN).

3 Homotopy analysis method

Liao [35] was the first to described HAM and successfully applied to compute the solution of the nonlinear differential equations. Initial guesses for the dimensionless equations are given below:

$$f_0(\zeta) = \alpha\left(\frac{1 - n^*}{1 + n^*}\right) + 1 - \exp(-\zeta),$$
$$\theta_0(\zeta) = \exp(-\zeta), \quad \phi_0(\zeta) = \exp(-\zeta), \quad (22)$$

and with the auxiliary linear operators as

$$L_f(f) = \left(\frac{d^3}{d\zeta^3} - \frac{d}{d\zeta}\right)f, \quad L_\theta(\theta) = \left(\frac{d^2}{d\zeta^2} - 1\right)\theta,$$
$$L_\phi(\phi) = \left(\frac{d^2}{d\zeta^2} - 1\right)\phi.$$
$$(23)$$

with the property that

$$L_f\left(K_1 + K_2 \exp(-\zeta) + K_3 \exp(\zeta)\right) = 0,$$
$$L_\theta\left(K_4 \exp(-\zeta) + K_5 \exp(\zeta)\right) = 0, \quad (24)$$

and

$$L_\phi\left(K_6 \exp(-\zeta) + K_7 \exp(\zeta)\right) = 0. \quad (25)$$

where $K_i (i = 1 \ldots 7)$ are constants and evaluated by the BCs.

The solution obtained by the HAM is given by

$$f_m(\zeta) = f_m^*(\eta) + \Gamma_1 + \Gamma_2 e^{-\zeta} + \Gamma_3 e^\zeta, \quad (26)$$

$$\theta_m(\zeta) = \theta_m^*(\zeta) + \Gamma_4 e^{-\zeta} + \Gamma_5 e^\zeta, \quad (27)$$

$$\phi_m(\zeta) = \phi_m^*(\zeta) + \Gamma_6 e^{-\zeta} + \Gamma_7 e^\zeta. \quad (28)$$

4 Results and discussions

The HAM contributes sovereignty to select the auxiliary parameters and these parameters have noticed remarkable concurrence in regulating and adjusting the convergence region. For the present problem to find the convergence region, the $\hbar$-curve were presented at the 15th terms. Figure 2 displays precisely the range of the permissible value of $\hbar_f$ and $\hbar_\theta$ are $-1.65 \leq \hbar_f \leq -0.55$, $-1.8 \leq \hbar_\theta \leq -0.42$ and $-1.74 \leq \hbar_\phi \leq -0.48$. the convergence of the solution are taken as $\hbar_f = \hbar_\theta = \hbar_\phi - 0.82$.

Also Table 1 indicates that the convergence of the HAM solution for several iterations. In Table 2, comparative investigation has been reported for the Rashidi et al. [45] and others with the present result (HAM). Numerical results for the SFC, NN and SN for various parameters are determined in Table 3.

Influences of the Magnetic parameter M, Prandtl Number Pr, radiation parameter R_d, Fluid parameter β, Index parameter n^*, Thermophoresis parameter N_t, BMP N_b, Deborah number in terms of thermal and concentration relaxation parameters De_1 and De_2 respectively, Schmidt number Sc and Wall temperature θ_w on the velocity, temperature and Nano concentration profiles are investigated in the form of graphs given by Figs. 3, 4, 5, 6, 7, 8, 9, 10, 11, 12, 13, 14, 15, 16, 17, 18, 19 and 20.

Figure 3 demonstrates the domination of index parameter n^* on the dimensionless velocity. Higher values of n enhances the stretching velocity followed by the higher rate of deformation in the fluid. Figure 4 portrays to show
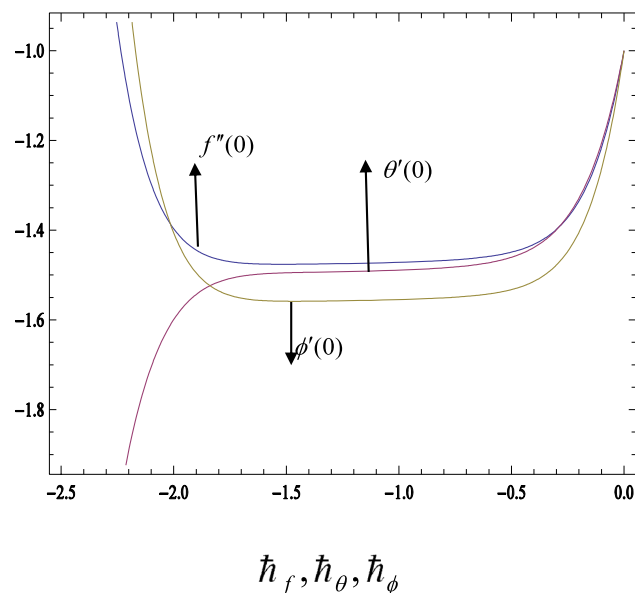
the consequence of wall thickness parameter α and velocity profile. Uplifting values of wall thickness, grounds in the increment to momentum boundary layer thickness and hence the velocity upsurges. Figure 5 plotted to carry out the inspection of non-Newtonian parameter β and velocity. Velocity profile goes higher with the growing effects of the parameter β. Physically enriching values of β, micro structure resistance due to material derivative increases and consequently the fluid viscosity decreases, leads to velocity enlarge. Figure 6 exhibits the effect of M on the profile f'.. Using Fig. 6, it is seen that enhancing values of M slows down the velocity of fluid in the boundary region. The purpose behindhand this phenomenon is that the uplifting values of M produces Lorentz force performed in contradiction of the velocity of the fluid in an electrically conducting area. The effect of temperature distribution against power index parameter and non-Newtonian parameter β are qualitative similar as shown in Figs. 7 and 8. Figure 9 demonstrates the impact of M on the temperature. The temperature increases as thermal boundary layer hikes. In Fig. 10, the impact of Thermophoresis parameter Nt with temperature profile is presented. It can be perceived that the hikes of Nt, the temperature profile is also hike ups. In Fig. 11, impacts of BM parameter Nb corresponding to the temperature profile is presented. We can see that as the value of BM parameter Nb hikes up, the mass diffusivity becomes

Table 1 Convergence of the HAM solutions for distinct order of iterations at $n^* = 0.5, M = 0.1, \hbar = -0.82, \beta_1 = 0.2, Pr = 1, \alpha = 0.2, De_1 = De_1 = 0.1, Sc = 1.1, \theta_w = 1, R_d = 0.1, N_t = 0.2 = N_b$

Approximations order	$-f''(0)$	$-\theta'(0)$	$-\phi'(0)$
1	0.71582	0.82478	0.69584
5	0.68451	0.81734	0.67120
10	0.67414	0.80285	0.66458
15	0.64125	0.78212	0.65379
20	0.63742	0.77189	0.64896
25	0.63742	0.77189	0.64896
30	0.63742	0.77189	0.64896

Table 2 Comparative discussion of the skin friction factor with the numerical techniques and present results for $\alpha^* = 0.5, M = \beta_1 = 0$.

n	Rashidi et al. [45]	Fang et al. [46]	Khader and Meghad [47]	Present (HAM)
0	0.9576443	0.9576	0.9576	0.95764211
0.5	0.9799497	0.9799	0.9798	0.97997652
1	1.0000084	1.0000	1.0000	1.00000000
2	1.0234206	1.0234	1.0234	1.02341876
3	1.0358835	1.0359	1.0359	1.03591048

$$\hbar_f, \hbar_\theta, \hbar_\phi$$

Fig. 2 Variation of $\hbar_f, \hbar_\theta$ and $\hbar_\phi$

Table 3 Numerical principles of SFC, the Nusselt number (NN) and the Sherwood number (SN) aimed at distinct parameters

n^*	α	β_1	M	Pr	θ_w	N_t	N_b	R_d	De_1	De_2	Sc	$f''(0)$	$\theta'(0)$	$\phi'(0)$
1	0.2	1	1	1	1	0.1	0.1	0.2	0.2	0.2	1	− 1.02457	− 0.75621	− 0.81232
1.2												− 1.04269	− 0.75160	− 0.81201
1.4												− 1.05317	− 0.75035	− 0.81002
1.6	0.3											− 1.11755	− 0.68521	− 0.76325
	0.5											− 1.13496	− 0.69330	− 0.76123
	0.7											− 1.16127	− 0.72319	− 0.77089
	1	1.1										− 1.25675	− 0.73598	− 0.77284
		1.2										− 1.24376	− 0.79664	− 0.80325
		1.3										− 1.22471	− 0.81273	− 0.84037
		1.5	1.2									− 1.08675	− 0.85231	− 0.83792
			1.4									− 1.09702	− 0.84120	− 0.83700
			1.6									− 1.12393	− 0.82078	− 0.82793
			2	3								− 1.23173	− 0.86705	− 0.84397
				5								− 1.24500	− 0.87221	− 0.84562
				7								− 1.52193	− 0.92176	− 0.96380
				0.71	1.5							− 1.34586	− 0.67848	− 0.83793
					1.7							− 1.34586	− 0.69741	− 0.84463
					1.9							− 1.34586	− 0.72996	− 0.85097
					2	0.3						− 1.08398	− 0.71861	− 0.75361
						0.5						− 1.08931	− 0.73510	− 0.79639
						0.7						− 1.08931	− 0.78869	− 0.84510
						0.8	0.2					− 1.18397	− 0.67413	− 0.72634
							0.4					− 1.19825	− 0.72741	− 0.76585
							0.6					− 1.20174	− 0.75557	− 0.77233
							0.7	0.4				− 1.13768	− 0.84538	− 0.76142
								0.6				− 1.08695	− 0.88579	− 0.76896
								0.8				− 1.05106	− 0.90425	− 0.77698
								1.0	0.6			− 1.07931	− 0.73655	− 0.78223
									0.8			− 1.08523	− 0.73655	− 0.78223
									1.0			− 1.12378	− 0.73655	− 0.78223
									1.1	0.3		− 1.15862	− 0.84320	− 0.74745
										0.4		− 1.15862	− 0.85379	− 0.74745
										0.5		− 1.15862	− 0.86413	− 0.74745
										0.7	1.3	− 1.10217	− 0.73981	− 0.69114
											1.5	− 1.10217	− 0.73924	− 0.76258
											1.7	− 1.10217	− 0.7289	− 0.78912

greater which paves the path to the increase temperature profile in the boundary layer area. Figure 12 is schemed for the Deborah number De_1 with temperature outline. Since De_1 resembles from the relaxation time because of heat flux. The higher Deborah number De_1 causes a lessening in the dimensionless temperature field and thickness of the boundary layer profile shrinks. Figure 13 portrays the consequences of radiation on velocity profile. It is very clear that the radiation parameter hikes up the velocity flow. Physically, a growth in the radiation discharges the heat to the flow which helps to hike up the thermal boundary layer thickness. Figure 14 depicted the wall temperature effects on temperature profile. When adiabatic wall temperature increases the distribution of the temperature in the case of heating generates a marked dilatation of the interaction region and shows a great augmentation in the
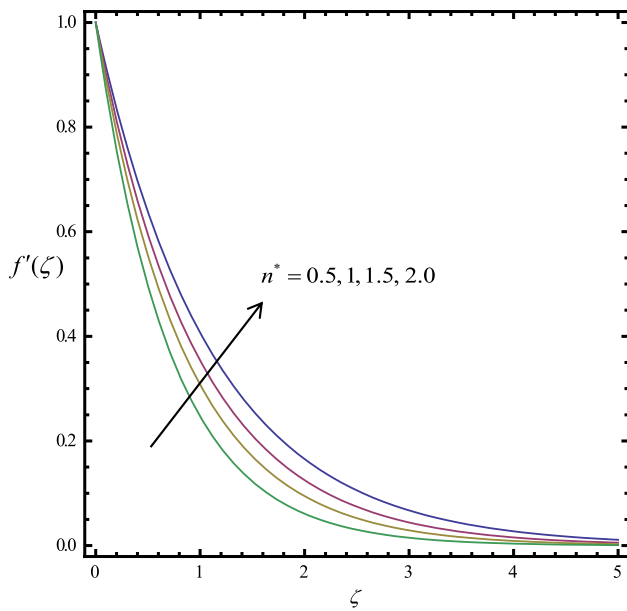
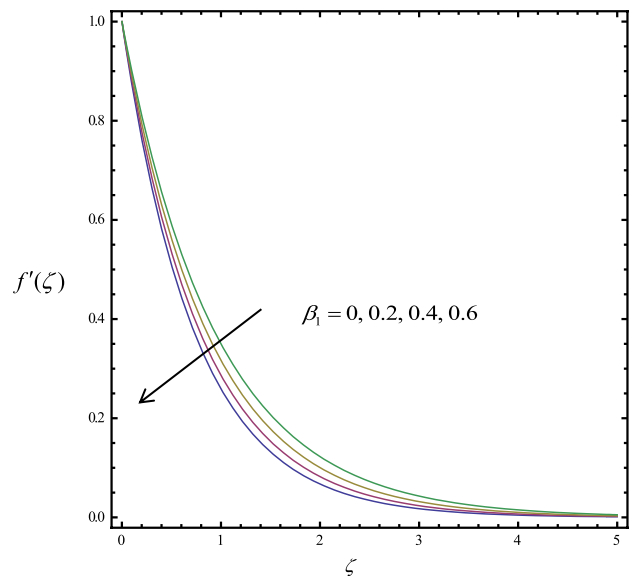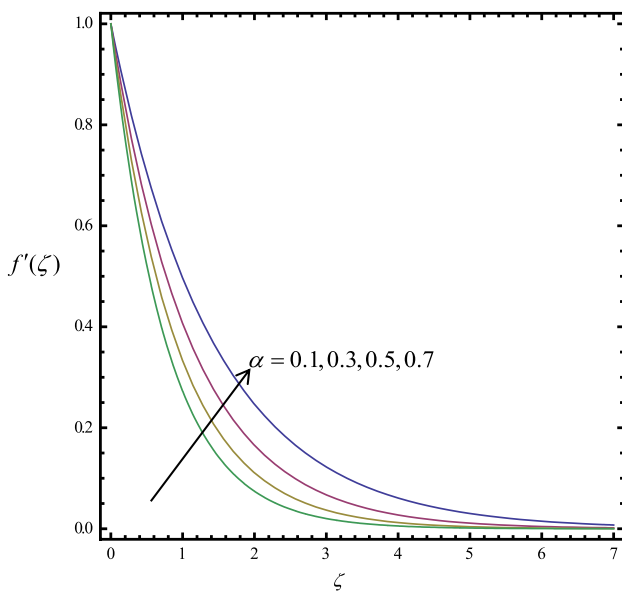**Fig. 3** Influence of index parameter n^* on velocity

Fig. 5 Influence of β on velocity

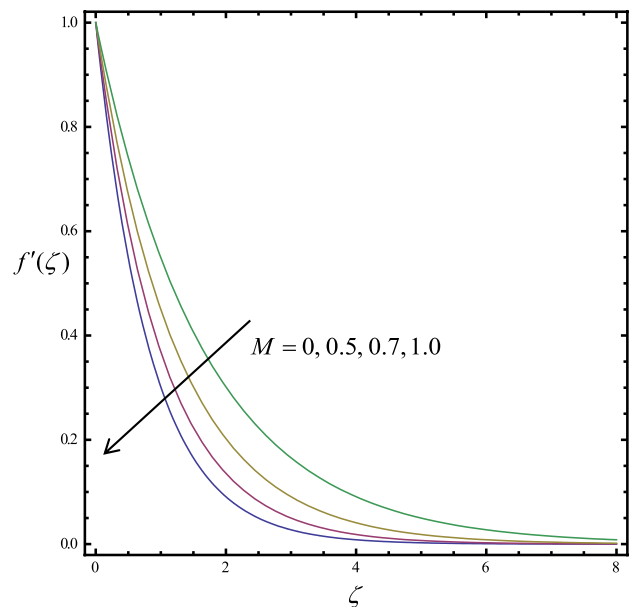**Fig. 4** Influence of wall thickness α on velocity

Fig. 6 Influence of magnetic parameter M on velocity

heat transfer. Figure 15 represents the consequences of PN with the temperature profiles. Prandtl number relates with the reversible thermal diffusivity. This grounds to decay in temperature distribution. Figure 16 represented the effect of nanoparticles concentration $\phi(\eta)$ and non-Newtonian parameter. Consequently the profile is decreases. In Fig. 17, responses of nanoparticles concentration with

thermophoresis parameter Nt is presented. It is noticed that the concentration profile hikes up with enhancement of Nt. Figure 18 represents the $\phi(\eta)$ for various value of Nb. We have observed that an hike of the value of Nb, pave the way to decrease the thermophoresis force. Subsequently the nanoparticles concentration profile reduces with
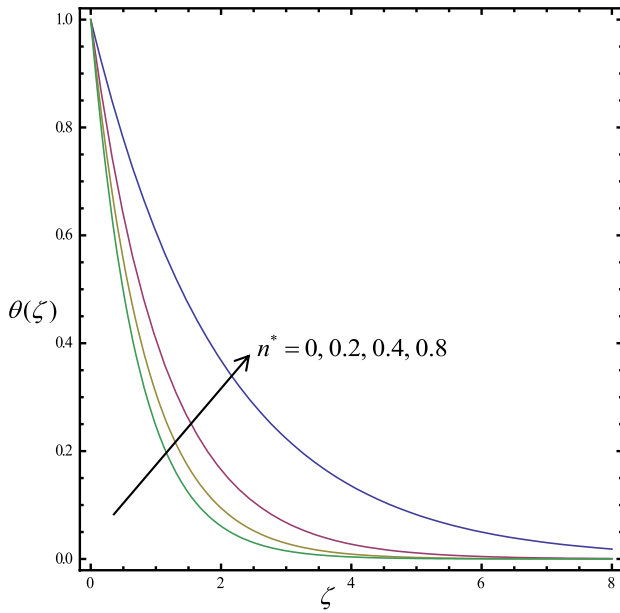
Fig. 7 Influence of index parameter n^* on temperature
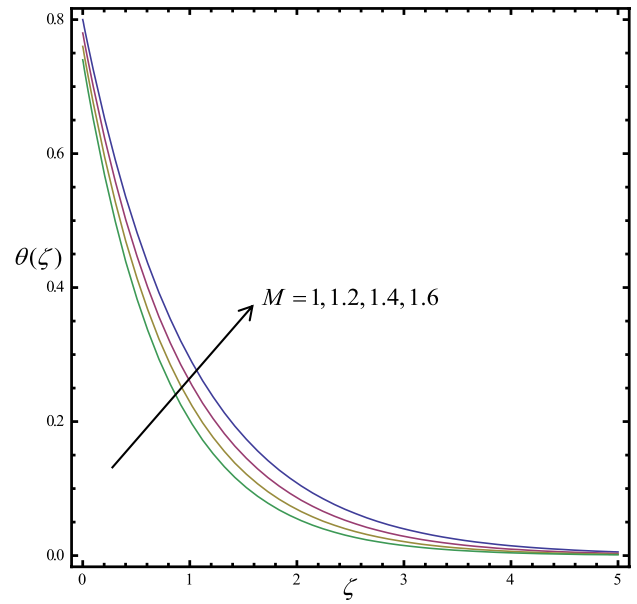
Fig. 9 Influence of magnetic parameter M on temperature
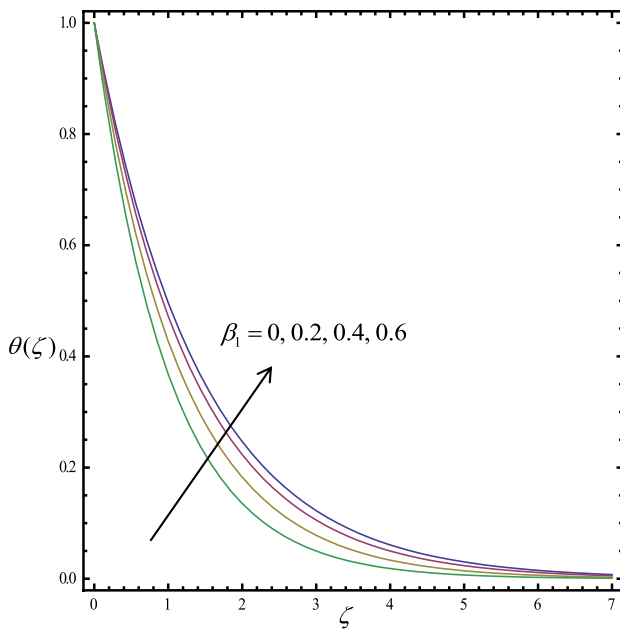
Fig. 8 Influence of β on temperature
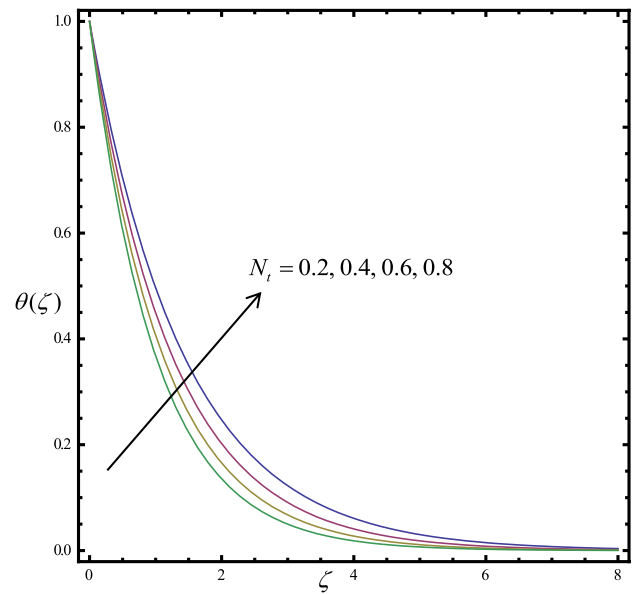
Fig. 10 Influence of Nt on temperature

the intensification of Nb. In Fig. 19 the consequences of Schmidt number Sc along with nanoparticles concentration profile is presented. A higher ideal of Schmidt number Sc resembles a depletion in the concentration profile. Last but not least the influence of Deborah number De_2 and

nanoparticles volume fraction were described in Fig. 20. Since De_2 corresponds from the relaxation time owing to mass flux. Higher values of De_2 causes a small penetration depth in concentration layer and in results reduction in the profile recorded.
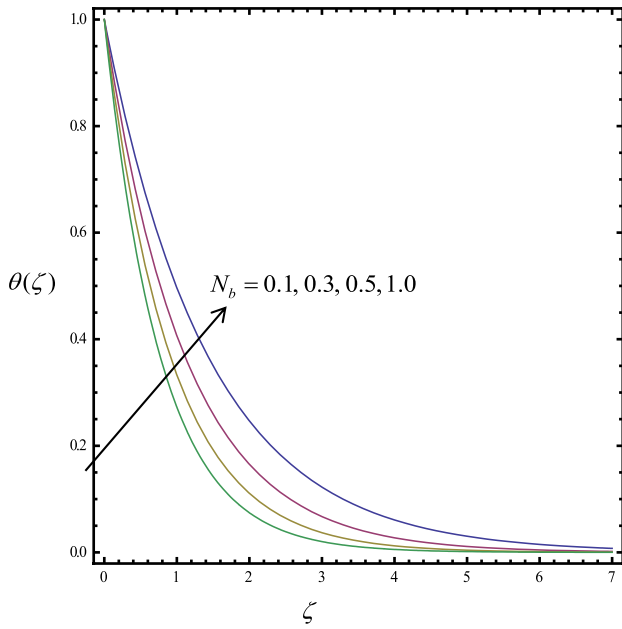
Fig. 11 Influence of *Nb* on temperature
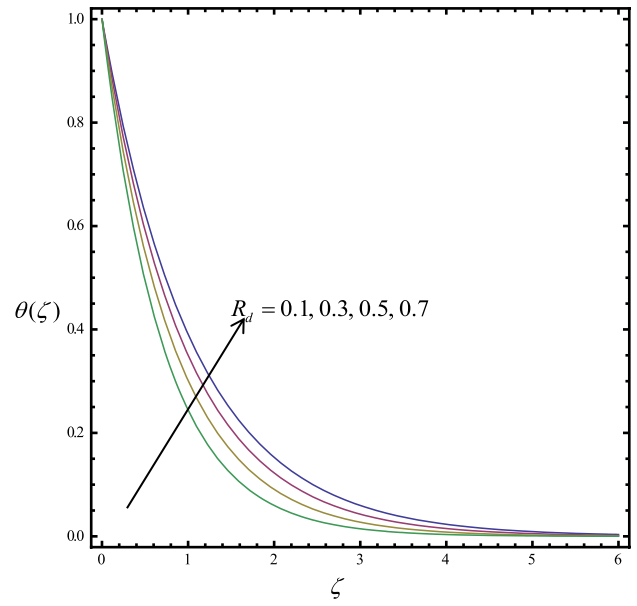
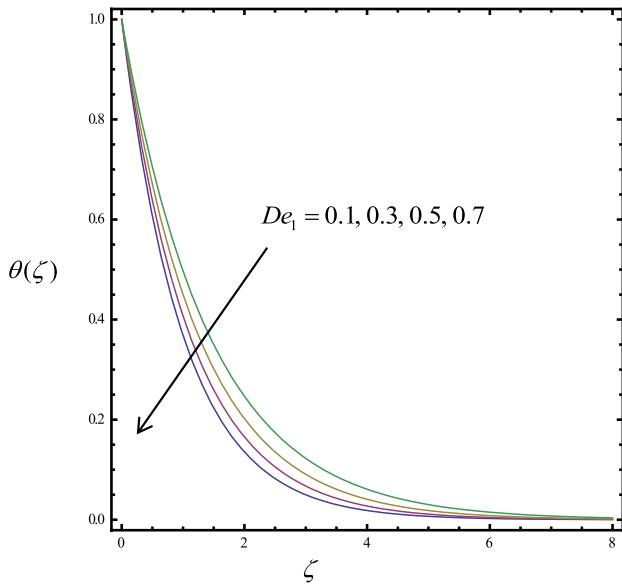**Fig. 13** Influence of *Radiation parameter R_d* on temperature

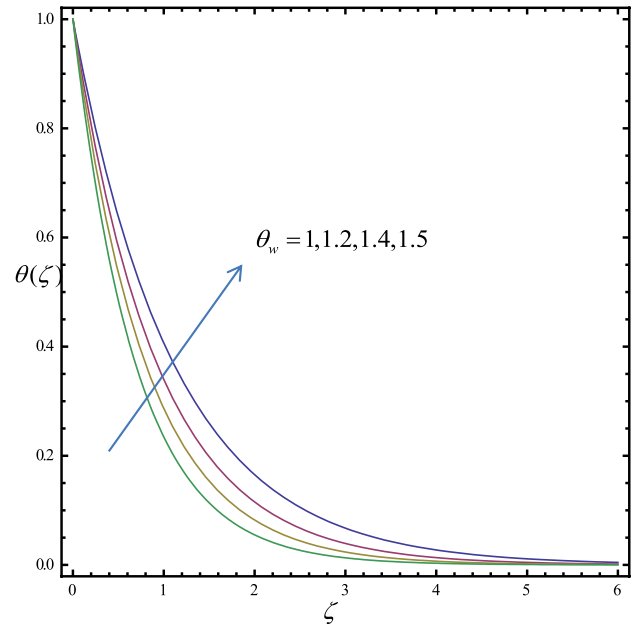**Fig. 12** Influence of *Deborah number De_1* on temperature

Fig. 14 Influence of *wall temperature parameter θ_w* on temperature
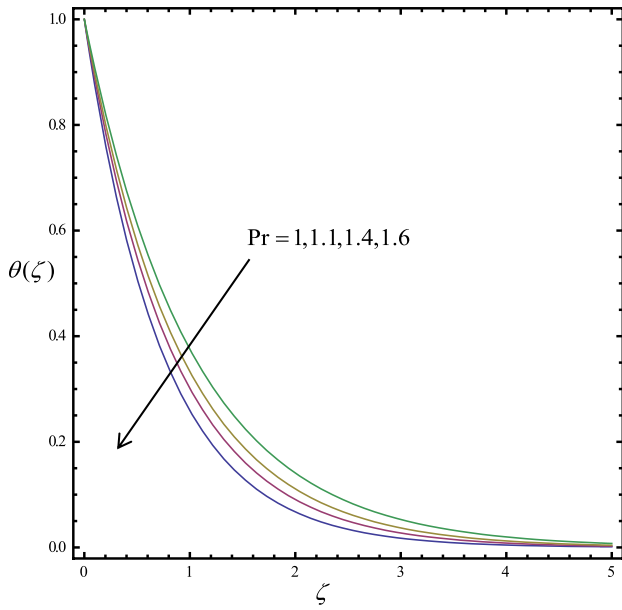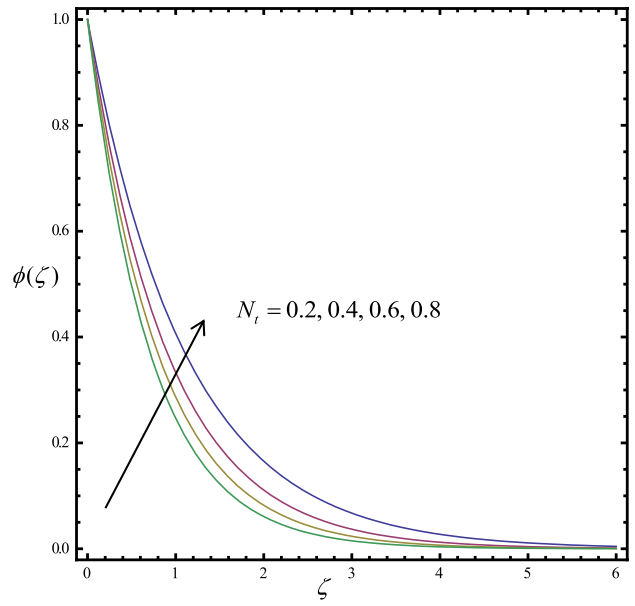
Fig. 15 Influence of Pr on temperature

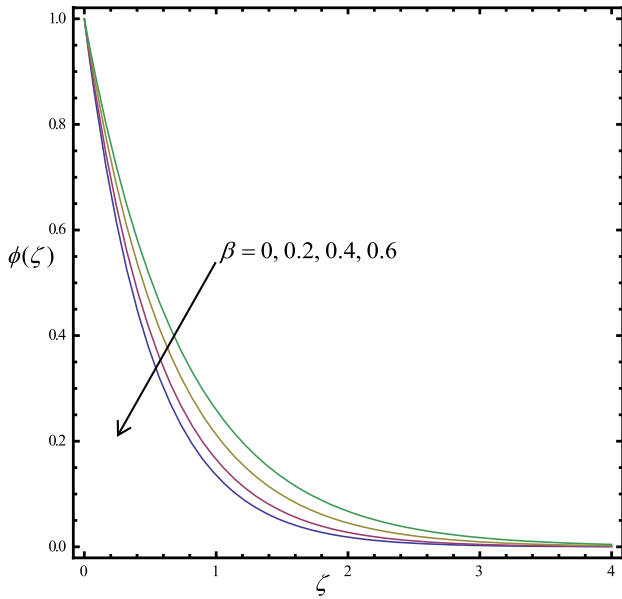Fig. 17 Influence of N_t on nanoparticles concentration

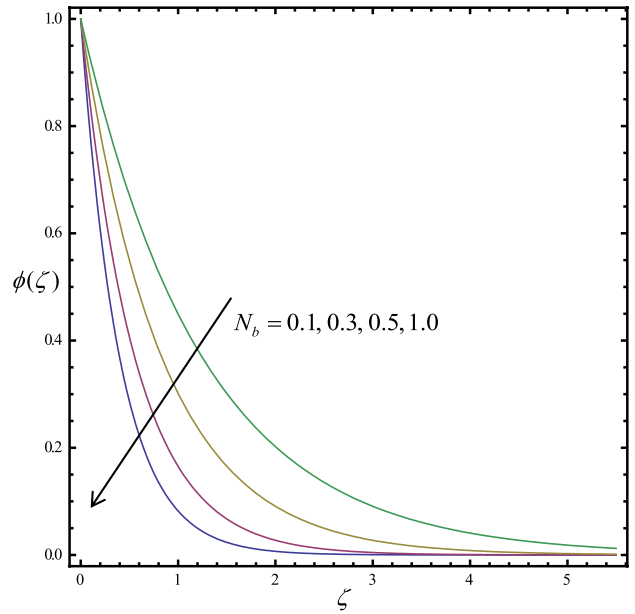Fig. 16 Influence of β on nanoparticles concentration

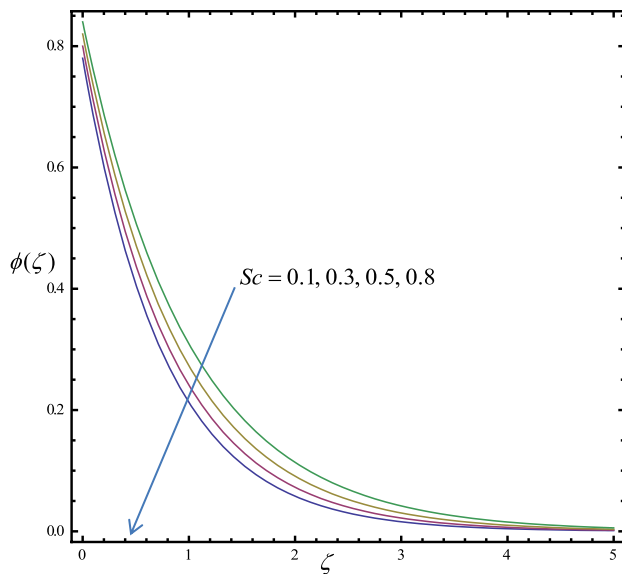

Fig. 18 Influence of N_b on nanoparticles concentration

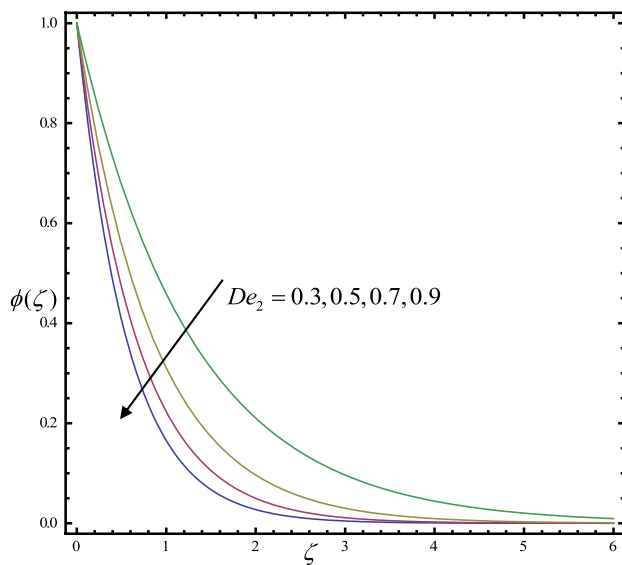**Fig. 19** Influence of Sc on nanoparticles concentration

Fig. 20 Influence of De_2 on nanoparticles concentration

5 Conclusions

Here, we discussed the magnetohydrodynamic two dimensional Williamson nanofluid flow over a stretching surface pertaining to the heat and mass transfer in the occurrence of nonlinear thermal radiation, Cattaneo–Christov heat and mass flux models, thermophoresis and Brownian motion. The transmuted equations of velocities, temperature and nano-profile are elucidated

analytically by HAM. High accuracy of the convergent series solution is handled by the Mathematica 9.0. A great agreement between HAM and existing results are demonstrated via tables. On the basis of contemporary examination the key outlines are as listed below:

- Accelerating values of index parameter n^* and wall thickness parameter α the horizontal fluid flow velocity promotes.
- Increasing values of M and β, the horizontal fluid velocity decreases.
- Temperature specie upsurges with rising of Nb, Nt, n^*, β, R_d, θ_w and M. Consequently demotes with the higher values of Pr and De_1.
- Nanoparticle volumetric specie escalates with the growing effects of Nt, while it diminishes with Nb, Sc and De_2.

Compliance with ethical standards

References

1. Choi SUS (1995) Enhancing thermal conductivity of fluids with nanoparticles. In: Developments and applications of non-Newtonian fluids. AJME, FED 231/MD, 66, 99105
2. Eastman JA, Choi US, Li S, Yuand W, Thompson LJ (2001) Anomalously increased effective thermal conductivities of ethylene glycol-based nanofluids containing copper nanoparticles. Appl Phys Lett 78:718–720
3. Das SK, Choi SUS, Yu W, Pradeep T (2007) Nanofluids: science and technology. Wiley, New York
4. Pak BC, Cho YI (1998) Hydrodynamic and heat transfer study of dispersed fluids with submicron metallic oxide particles. Exp Heat Transf 11:151–170
5. Eastman JA, Choi US, Li S, Yu W, Thompson LJ (1996) Enhanced thermal conductivity through the development of nanofluids. MRS Online Proc Libr Arch 457:1–10
6. Kim J, Kang YT, Choi CK (2004) Analysis of convective instability and heat transfer characteristics of nanofluids. Phys Fluids 16:2395–2401
7. Wang X, Mujumdar AS (2008) A review on nanofluids-part-I theoretical and numerical investigations. Braz J Chem Eng 25(4):613–620
8. Kakac S, Pramuanjaroenkij A (2009) Review of convective heat transfer enhancement with nanofluids. Int J Heat Mass Transf 52:3187–3196
9. Buongiorno J (2005) Convective transport in nanofluids. J Heat Transf 128(3):240–250
10. Das SK, Choi SU, Patel HE (2006) Heat transfer in nanofluids—a review. Heat Transf Eng 27:3–19
11. Khanafer K, Vafai K (2011) A critical synthesis of theromophysical characteristics of nanofluids. Int J Heat Mass Transf 54:4410–4428

12. Tiwari RK, Das MK (2007) Heat transfer augmentation in a two-sided lid-driven differentially heated square cavity utilizing nanofluids. Int J Heat Mass Transf 50:2002–2018

13. Oztop F, Abu-Nada E (2008) Numerical study of natural convection in partially heated rectangular enclosures filled with nanofluids. Int J Heat Fluid Flow 29:1326–1336

14. Wei X, Wang L (2010) Synthesis and thermal conductivity of microfluidic copper nanofluids. Particuology 8(3):262–271

15. Kuznetsov AV, Nield DA (2010) Natural convective boundary-layer flow of a nanofluid past a vertical plate. Int J Therm Sci 49(2):243–247

16. Nield DA, Kuznetsov AV (2013) The Cheng-Minkowycz problem for natural convective boundary layer flow in a porous medium saturated by a nanofluid: a revised model. Int J Heat Mass Transf 65:682–685

17. Kuznetsov AV, Nield DA (2011) The Cheng-Minkowycz problem for the double-diffusive natural convective boundary layer flow in a porous medium saturated by a nanofluid. Int J Heat Mass Transf 54:374–378

18. Khan WA, Pop I (2010) Boundary layer flow of nanofluid past a stretching sheet. Int J Heat Mass Transf 53:2477–2483

19. Khan WA, Aziz A (2011) Natural convection flow of a nanofluid over a vertical plate with uniform surface heat flux. Int J Therm Sci 50:1207–1214

20. Sheikholeslami M, Rezaeianjouybari B, Darzi M, Shafee A, Li Z, Nguyen TK (2019) Application of nano-refrigerant for boiling heat transfer enhancement employing an experimental study. Int J Heat Mass Transf 141:974–980

21. Sheikholeslami M, Jafaryar M, Shafee A, Li Z, Haq R (2019) Heat transfer of nanoparticles employing innovative turbulator considering entropy generation. Int J Heat Mass Transf 136:1233–1240

22. Sheikholeslami M (2019) New computational approach for exergy and entropy analysis of nanofluid under the impact of Lorentz force through a porous media. Comput Method Appl Mech Eng 344:319–333

23. Sheikholeslami M, Mahian O (2019) Enhancement of PCM solidification using inorganic nanoparticles and an external magnetic field with application in energy storage systems. J Clean Prod 215:963–977

24. Sheikholeslami M, Arabkhoosar A, UlHaq R, Shafee A, Li Z (2019) Impact of Lorentz forces on Fe_3O_4–water ferrofluid entropy and exergy treatment within a permeable semi annulus. J Clean Prod 221:885–898

25. Sheikholeslami M, Shafee A, Zareei A, UlHaq R, Li Z (2019) Heat transfer of magnetic nanoparticles through porous media including energy analysis. J Mol Liq 279:719–732

26. Jha BK, Malwgi PB (2019) Combined effects of hall and ion-slip current on MHD free convection flow in a vertical micro-channel. SN Appl Sci 1:1163–1175

27. El Dabe NT, Attia HA, Essawy MAI, Abd-Elmaksoud IH, Ramadan AA (2019) Non-linear heat and mass transfer in a thermal radiated MHD flow of a power-law nanofluid over a rotating disk. SN Appl Sci 1:551–561

28. Kumar KA, Sugunamma V, Sandeep N, Reddy JVR (2019) MHD stagnation point flow of Williamson and Casson fluids past an extended cylinder: a new heat flux model. SN Appl Sci 1:705–716

29. Hayat T, Naseem A, Khan MI, Farooq M, Alsaedi A (2017) Magnetohydrodynamic flow of nanofluid with double stratification and slip condition. Phys Chem Liq 55:1–20

30. Hayat T, Rashid M, Imtiaz M, Alsaedi A (2016) Magnetohydrodynamic (MHD) flow of Cu-Water nanofluid due to rotating disk with partial slip. AIP Adv 1:1–11

31. Mabood F, Shateyi S, Rashidi MM, Momoniat E, Freidoonimehr F (2016) MHD stagnation point flow heat and mass transfer of nanofluids in porous medium with radiation, viscous dissipation and chemical reaction. Adv Powder Technol 27:742–749

32. Hayat T, Muhammad T, Shehzad SA, Chen GQ, Abbas IA (2015) Interactive of magnetic field in flow of Maxwell nanofluid with convective effect. J Magn Magn Mater 389:48–57

33. Shehzad SA, Abdullah Z, Abbasi FM, Hayat T, Alsaedi A (2016) Magnetic field effects in three dimensional flow of an Oldroyd B nanofluid over a radiative surface. J Magn Magn Mater 399:97–108

34. Shehzad SA, Hayatand T, Alsaedi A (2015) Influence of convective heat and mass conditions in MHD flow of nanofluid. Bull Pol Acad Sci Technol 63:465–474

35. Farooq U, Zhao YL, Liao SJ (2015) Application of HAM- based Mathematica package BVPh 2.0 on MHD Falkner–Skan flow of nanofluid. Comput Fluids 111:69–75

36. Hayat T, Muhammad T, Shehzad SA, Alsaedi A (2017) Three dimensional rotating flow of Maxwell nanofluid. J Mol Liq 229:495–500

37. Hayat T, Muhammad T, Shehzad SA, Alsaedi A (2017) An analytical solution for magnetohydrodynamic Oldroyd B nanofluid flow induced by a stretching sheet with heat generation/absorption. Int J Therm Sci 111:274–288

38. Gupta S, Sharma K (2017) Numerical simulation for magnetohydrodynamic three dimensional flow of Casson nanofluid with convective boundary conditions and thermal radiation. Eng Comput 34(8):2698–2722

39. Gupta S, Kumar D, Singh J (2018) MHD mixed convective stagnation point flow and heat transfer of an incompressible nanofluid over an inclined stretching sheet with chemical reaction and radiation. Int J Heat Mass Transf 118:378–387

40. Gupta S, Sharma K (2017) Mixed convective MHD flow and heat transfer of uniformly conducting nanofluid past an inclined cylinder in presence of thermal radiation. J Nanofluids 6(6):1031–1045

41. Sharma K, Gupta S (2017) Viscous dissipation and thermal radiation effects in MHD flow of Jeffrey nanofluid through impermeable surface with heat generation/absorption. Nonlinear Eng 6(2):153–166

42. Sharma K, Gupta S (2018) Radiation effects on MHD boundary layer flow and heat transfer along a stretching cylinder with variable thermal conductivity in a porous medium. J Porous Med 21:763–779

43. Sharma K, Gupta S (2017) Homotopy analysis solution to thermal radiation effects on MHD boundary layer flow and heat transfer towards an inclined plate with convective boundary conditions. Int J Appl Comput Math 3(3):2533–2552

44. Liao SJ (2012) Homotopy analysis method in nonlinear differential equation. Springer, Heidelberg

45. Reddy S, Naikote K, Rashidi MM (2017) MHD flow and heat transfer characteristics of Williamson nanofluid over a stretching surface with variable thickness and variable thermal conductivity. Trans A Razmade Math Inst 171:195–211

46. Fang T, Zhang J, Zhong Y (2012) Boundary layer flow over a stretching sheet with variable thickness. Appl Math Comput 218:7241–7252

47. Khader MM, Meghad AM (2013) Numerical solution for boundary layer flow due to nonlinear stretching sheet with variable thickness and slip velocity. Eur Phys J Plus 128:100–112